Ceramics-Silikáty 67 (1), 120-134 (2023)
www.ceramics-silikaty.cz doi: 10.13168/cs.2023.0009

EVALUATION OF THE POTENTIAL OF BARIUM ZIRCONATE ON THE SINTERABILITY AND PROPERTIES OF BOVINE HYDROXYAPATITE

#SULEYMAN SERDAR PAZARLIOGLU*, SEDA ATAS BAKDEMIR**, HASAN GOKCE***
*Marmara University, Technology Faculty, The Department of Metallurgy and Materials Engineering, Recep Tayyip Erdogan Campus, 34854, Maltepe, Istanbul, Turkey
**National Defense University, Naval Academy, Tuzla, Istanbul, Turkey
***Istanbul Technical University Prof. Dr. Adnan Tekin Materials Research Center ITU Ayazaga Campus Maslak Sarıyer-Istanbul, Turkey

#E-mail: spazarlioglu@marmara.edu.tr

Submitted January 23, 2023; accepted March 1, 2023

Keywords: Bovine hydroxyapatite, Barium zirconate, Sintering performance, Properties

In the present study, the potential of barium zirconate ($BaZrO_3$; 1-5 wt. %) on the sinterability, and properties of bovine hydroxyapatite (BHA) was evaluated. BHA decomposed into beta and alpha-tricalcium phosphate (β and α-TCP) at a 4.7 % rate. Tetracalcium phosphate (TTCP) was detected as the decomposition phase in the $BaZrO_3$ added BHAs, and it increased up to 10.7 % with an increasing $BaZrO_3$ ratio. In addition to TTCP, the phases of $BaZrO_3$, Ba_2ZrO_4, σ-$Ba_2P_2O_7$, $Ba_3P_2O_8$ and $CaZrO_3$ were detected in the composites. The addition of $BaZrO_3$ at an amount of 3 wt. % has a higher potential than the others to improve the sinterability and properties of BHA. It contributed to the increase in the fracture toughness from 0.99 ± 0.13 to 1.80 ± 0.12 MPa·m$^{1/2}$ and the compressive strength from 115.75 ± 4.27 to 173.66 ± 13.61 MPa, and the decrease in the brittleness index from 4.24 ± 0.31 to 2.45 ± 0.15 μ$^{-1/2}$. The in-vitro bioactivity of BHA also increases with the additional $BaZrO_3$. However; it is recommended to be used in applications that do not require load bearing in the human body due to its insufficient fracture toughness.

INTRODUCTION

Currently, implants are extensively applied for the medical treatment of skeletal injuries, degenerative bones, and decaying teeth. Among the ceramic materials, hydroxyapatite ($Ca_{10}(PO_4)_6(OH)_2$, HA) is widely used in various medical applications due to its chemical composition being similar to the mineral part of teeth and human bones [1]. HA does not cause any stimulating and repulsive effects when added into the human body. Moreover, HA can combine with the original bone tissue to form a solid bone [2]. It can be synthesised chemically or extracted from biological sources [3]. Biological HA contains different kinds of cationic and anionic impurities. These ionic impurities in biological HAs could be a reason for its better biocompatibility than synthetic HAs [4]. Therefore, many works have been devoted to the development of HA from biological sources like camel bones [5], chicken bones [6], goat bones [7], pork bones [8], sheep bones [9], and bovine bones [10]. Studies on bovine bone hydroxyapatite (BHA) produced in powder and granule forms have shown that it can be used for the treatment of maxillary sinus augmentation [11], alveolar bone loss [12], restorative biomaterial for dental implants [13], and bone replacement [14]. A literature survey showed that BHA had a maximum density of 2.72 ± 0.01 g·cm^{-3} [15], a maximum compression strength of 75.20 ± 18.30 MPa [16] and a maximum hardness of 337.90 ± 12.12 $HV_{0.2}$ [17]. Therefore, it does not have enough mechanical reliability for use in the human body. Numerous studies have been conducted to improve its mechanical reliability by introducing different ceramic materials as shown in Table 1.

An implant material planned for load-bearing applications in the human body should have a compressive strength between 100-230 MPa, and a fracture toughness between 2-6 MPa·m$^{1/2}$ [32]. A literature survey shows that BHA-composites, except those doped with perovskite-type ceramic materials, i.e., $CaTiO_3$, and $LiAlO_2$, do not have high enough mechanical reliability to be used for load-bearing applications in the human body. Perovskites are a group of functional materials generally described with the ABX_3 formula [33]. Among the ABO_3-type perovskites, $BaZrO_3$ (barium zirconate) has several technological applications in many different areas due to its superior properties, such as a high dielectric constant (430 at 25 °C), low thermal expansion point (α = 8.7 ×10^{-6}/°C), high chemical stability, high melting point (~3000 K) [34]. These properties make $BaZrO_3$ suitable as a solid electrolyte in fuel cells, humidity sensors, microwave applications, wireless communications as electro-ceramic capacitors, etc [35]. In addition, $BaZrO_3$ is an alternative material for yttria-stabilised zirconia as a thermal barrier coating material in the aerospace

industry for supersonic jets [36]. It is also used as a coating material on the surface of metallic [37], and ceramic [38] materials and as an additive material to $0.775Na_{0.5}Bi_{0.5}TiO_{3-0.225}BaSnO_3$ [39], $NdBa_2Cu_3O_{7-\delta}$ [40], $Ba_2Cu_3O_{7-x}$ [41], $YBa_2Cu_3O_{7-\delta}$ [42] alloys. However, there is no study on its potential as an additive material to BHA.

In this study, BHA with and without $BaZrO_3$ additives was sintered at 900 °C, 1000 °C, 1100 °C, 1200 °C, and 1300 °C for 4 h to investigate the potential of $BaZrO_3$ on the properties of BHA. The resultant samples were characterised using shrinkage, density, porosity, hardness, fracture toughness, brittleness index, compression strength, X-ray diffraction (XRD), and scanning electron microscopy (SEM).

EXPERIMENTAL

Materials and Methods

In the present study, BHA powders were derived from bovine bones according to our previous study [31].

Table 1. Highest properties achieved in BHAs with various reinforcing materials (D: Density, H: Hardness, S: Strength, Kıc: Fracture toughness, BI: Brittleness Index, P: Porosity).

Reinforcement materials and amounts in BHA matrix	Property	Reference
TiO_2 (5, and 10 wt. %)	H: 247.40 ± 11.45 $HV_{0.2}$ S: 109.47 ± 3.58 MPa	[18]
CeO_2 (1-10 wt. %)	D: 2.879 g·cm^{-3} S: 107 MPa	[18]
Li_2O (0.25-2 wt. %)	D: 2.844 g·cm^{-3} H: 174 $HV_{0.2}$ S: 75.4 MPa	[20]
20 wt. % TCP – 10 wt. % MgO	H: 2.5 GPa S: 110 MPa	[21]
La_2O_3 (0.25-2 wt. %)	H: 287.1 ± 20.00 $HV_{0.2}$ S: 88.84 ± 3.99 MPa	[22]
Y_2O_3 (0.5, and 1 wt. %)	D: 2.94 ± 0.13 g·cm^{-3} H: 672.4 ± 94.8 $HV_{0.2}$ S: 81.84 ± 27.01 MPa	[23]
ZrO_2 (5, and 10 wt. %)	D: 2.94 ± 0.13 g·cm^{-3} H: 166 ± 2 $HV_{0.2}$ S: 50 ± 10 MPa	[24]
Mullite (5-12.5 wt. %)	D: 2.766 g·cm^{-3} H: 369.4 $HV_{0.2}$ S: 118 MPa	[25]
Borosilicate glass (5, and 10 wt. %)	D: 2.84 ± 0.12 g·cm^{-3} H: 232.95 ± 22.15 $HV_{0.2}$ S: 117.17 ± 15.98 MPa	[26]
SrO (5, and 10 wt. %)	D: 3.2058 g·cm^{-3} H: 257.4 ± 29.67 $HV_{0.2}$ S: 19.85 ± 3.33 MPa	[27]
B_2O_3 (5-10 wt. %)	H: 249.5 ± 62.9 $HV_{0.2}$ S: 39.91 ± 14.4 MPa	[28]
Commercial Inert Glass (5-10 wt. %)	D: 2.63 ± 0.06 g·cm^{-3} H: 506.5 ± 67.85 $HV_{0.2}$ S: 132.98 ± 29.37 MPa	[29]
$CaTiO_3$ (5-10 wt. %)	D: ≈ 2.9 g·cm^{-3} H: ≈ 4.5 GPa P: ≈ 1% K_{ic}: ≈ 4.5 MPa·m$^{1/2}$	[30]
$LiAlO_2$ (1-5 wt. %)	D: 2.832 ± 0.003 g·cm^{-3} H: 3.63 ± 0.26 GPa S: 218 ± 14.02 MPa K_{ic}: 1.95 ± 0.18 MPa·m$^{1/2}$ BI: 2.09 ± 0.38 μ$^{-1/2}$	[31]

BHA and $BaZrO_3$ (99.99 % in purity; Merck, USA, separately, in amounts of 1, 3, and 5 wt. %) powders were mixed and then homogenised for 4 h at 200 rev/min (rpm) in a ball milling device. BHA and the composite powders at a weight of 2.0 g were pelleted using a uniaxial press at 350 MPa. Before the sintering treatments, the pelleted samples were dried at 105 °C for 1 day, and they were sintered in air condition between 900 °C and 1300 °C for 4 h at heating and cooling rates of 5 °C.

The physical properties of BHA with and without the $BaZrO_3$ additives were calculated using shrinkage, density, porosity, and relative density measurements. The shrinkage rates were calculated by comparing the thickness of each sample before and after the sintering process with electronic callipers which have 1/1000 sensitivity as shown in Equation 1.

$$S = \frac{H_0 - H_1}{H_0} \times 100 \quad (1)$$

where S is the shrinkage (%), H_0 is the thickness before sintering (mm), and H_1 is the thickness after sintering (mm).

The sintered densities (d) and porosities (p) of the bulk samples were determined using the Archimedes method in distilled water as the immersing medium using Equations 2, and 3, respectively.

$$d_s = \frac{M_k}{M_a - M_s} \quad (2)$$

$$p = \left(\frac{M_a - M_k}{M_a - M_s}\right) \times 100 \quad (3)$$

where ds is the sintered density ($g \cdot cm^{-3}$), p is the porosity (%), M_k is the dry weight, M_a is the wet weight of the sample and M_s is the wet weight of the suspension in distilled water.

The relative density of the composites was calculated by dividing the sintered density by the theoretical density of each composite, determined using the rule of mixture [43], and using the values of 3.156 $g \cdot cm^{-3}$ for BHA [44], and 5.960 $g \cdot cm^{-3}$ for $BaZrO_3$ [45], respectively. The mechanical properties of BHA with and without the $BaZrO_3$ additives were calculated using hardness, fracture toughness, brittleness index, and compression strength measurements. For the hardness and fracture toughness measurements, the samples were ground with SiC paper (between 800 and 5000 mesh) and then polished with a diamond paste (between 10 and 1 μm) to obtain mirror-like surfaces. The hardness of the polished samples was analysed utilising a microhardness tester (Future Tech FM 301, Japan) with a Vickers indenter with an application load of 1.962 N and a dwell time of 20 s because it provided the formation of a hardness indent without cracking. Equation 4 was used to calculate the HV (GPa), where F is the applied load (N), and d is the length of the indent (mm).

$$HV = 0.0001854 \frac{F}{d^2} \quad (4)$$

In order to calculate the fracture toughness, a load of 2.943 N was used for a dwell time of 10 s, which was determined by Equation 5. For the radial crack length measurement, optical images of the indents were taken.

$$K_{Ic} = 0.203 \left(\frac{c}{a}\right)^{-1.5} HV\, a^{0.5} \quad (5)$$

where K_{IC} is the fracture toughness, c is the radial crack dimension measured from the centre of the indent impression (m), and a is the half diagonal of the indentation (m).

Ten samples were used to calculate the compressive strength of the pure BHA and each composite, which was determined at a loading rate of 2 $mm \cdot min^{-1}$ with a Universal tester (Devotrans FU 50 kN, Turkey). Equation 6 was employed to calculate the brittleness index [46] of the samples, where B is brittleness index, HV is the hardness, and K_{Ic} is the fracture toughness.

$$B = \frac{HV}{K_{Ic}} \quad (6)$$

The phases that occurred during the sintering process in the samples were analysed by a Philips X'Pert X-ray diffraction machine using Cu-Kα as the radiation source at a scan speed of 0.6° per minute and a step scan of 0.02° in the range of 2θ values between 20° and 50°. The percentage of the phases was determined by Rietveld analysis. The changes in the surface morphology of the sintered samples were determined by an FEI Sirion XL30 SEM machine. The average grain size of the sintered samples was determined by the linear intercept method.

The samples with high mechanical properties were ground with SiC papers of up to 1200 mesh and rinsed ultrasonically in acetone, absolute alcohol and deionised water in turn five times to remove any contamination and particulates. The solution was prepared by dissolving reagent grade sodium chloride (NaCl), potassium chloride (KCl), calcium chloride dihydrate ($CaCl_2 \cdot 2H_2O$), magnesium chloride hexahydrate ($MgCl_2 6H_2O$), sodium hydrogen carbonate ($NaHCO_3$), dipotassium hydrogen phosphate trihydrate ($K_2HPO_4 3H_2O$), sodium sulfate (Na_2SO_4) in deionised water. Then the solution was buffered to a physiological pH of 7.32 at 37 ± 1 °C by both hydrochloric acid (HCl) and tris (hydroxymethyl) aminomethane ($(CH_2OH)_3CNH_2$). The *in vitro* bioactivity was evaluated by soaking the pellets mounted vertically, in 40 mL of simulated body fluid (SBF) prepared according to Ref [47] for 14 and 28 days. After immersion in the SBF for various periods, the immersed samples were retrieved, gently rinsed with distilled water, and dried at 60 °C for 1/2 day. The SEM analysis finally examined the surface of the samples, and the Ca/P ratio was calculated by energy dispersive X-ray diffraction (EDS) analysis.

RESULTS AND DISCUSSION

The XRD patterns of BHA without the $BaZrO_3$ additive are shown in Figure 1. The HA stability was not disrupted when BHA was sintered up to 1000 ºC, and all the XRD peaks up to this temperature are in good agreement with a characteristic pattern of HA. However, it decomposed to beta-tricalcium phosphate (β-TCP) at an amount of 3.3 % when sintering was carried out at 1100 °C. Sintering at 1200 °C caused an increase in the amount of β-TCP from 3.3 % to 3.4 % and the formation of alpha-tricalcium phosphate (α-TCP) at about 0.3 % was detected. When sintering was performed at 1300 °C, the amount of β- and α-TCP increased to 3.9 % and 0.8 %, respectively. The decomposition rate measured at 1300 °C for BHA at 4.7 % in the present study is about 32% less than that of Ref [48], and it has a suitable decomposition rate for use in the human body according to the ISO 13779-3:2018 standard [49]. If the sintering temperature of BHA reaches ≈1200 °C, the initial biphasic mixture of HA + β-TCP transforms into a triphasic HA + β-TCP +α-TCP formulation [50]. This combination has great potential for enhancing the bioactivity and bone regeneration capabilities compared to a biphasic mixture of HA + β-TCP. The presence of the α-TCP phase in the three-phase HA + β-TCP + α-TCP formulation significantly increases the *in vitro* bioactivity, allowing the better control over the bioactivity and biodegradation of BHA implants [51].

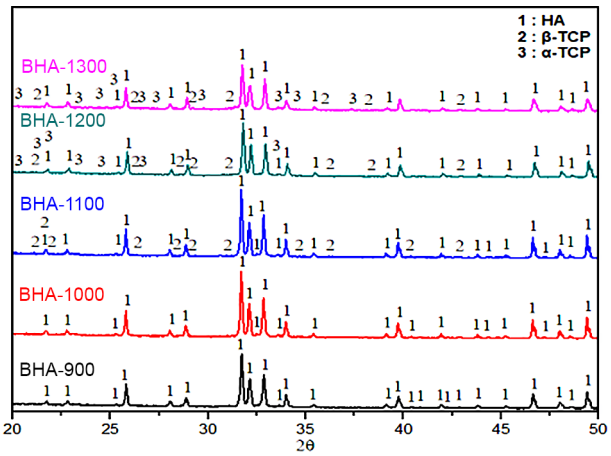

Figure 1. XRD patterns of the pure BHA with the $BaZrO_3$ additive depending on the sintering temperatures.

Figure 2 shows the XRD patterns of the BHA-$BaZrO_3$ composites. It is observed that HA and $BaZrO_3$ can be detected at temperatures of 900 and 1000 °C, regardless of the $BaZrO_3$ ratio in the composites. When sintering is performed at and above 1100 °C, the sintered samples consist of several phases such as $BaZrO_4$, Sigma-$Ba_2P_2O_7$, $Ba_3P_2O_8$, $CaZrO_3$ and tetracalcium phosphate (TTCP). It is well documented in the literature that temperatures higher than 1000 °C are necessary for

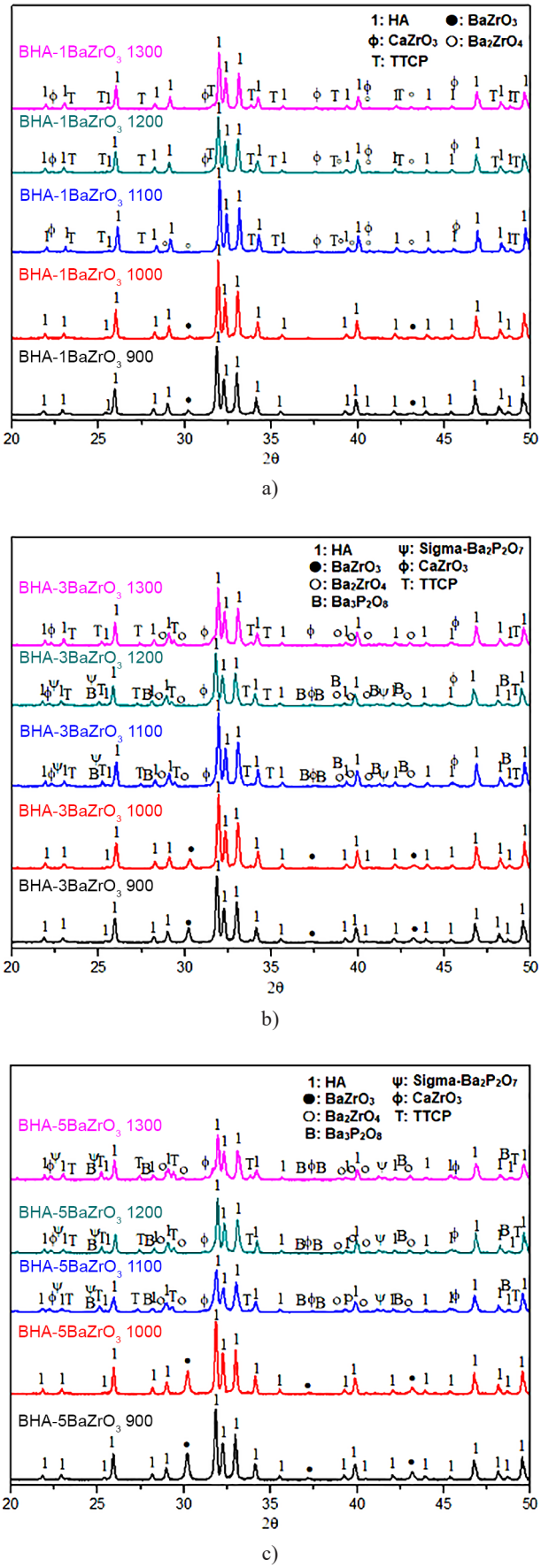

Figure 2. XRD patterns of BHA-$BaZrO_3$ composites.

the formation of these phases. As stated by Róg et al., Ba_2ZrO_4 occurs between 1100 and 1300 °C after the peritectic transformation of L+$Ba_2Zr_3O_7$ in the BaO–ZrO_2 binary system [52]. $Ba_2Zr_3O_7$ was not detected in the present study because it is formed at 1375 °C [53]. Sigma-$Ba_2P_2O_7$ and $Ba_3P_2O_8$ are in the family of alkaline earth phosphates with the general formula $A_2P_2O_7$, $A_3(PO_4)_2$, $A_7P_4O_{17}$, $A_4(PO_4)_2O$ etc. [54]. $Ba_2P_2O_7$ has two different crystal structure types: α-type, a low-temperature phase (Orthorhombic: P_{nma}), and σ-type: a high-temperature phase (hexagonal: P-6_{2m}) [55]. Adding $BaZrO_3$ and $Ba_2P_2O_7$ as a filler enhances the radiation shielding property of the Polipol 314-filled polyester resin used in nuclear medicine [56]. $Ba_3P_2O_8$ is non-toxic [57], and it can be used for the removal of methyl blue (MB), which damages the skin, eyes, and mucous membrane of humans [58]. The TTCP detected in $BaZrO_3$ added BHAs is a reliable CaP compound with excellent biocompatibility, and osteoconductivity [59]. It was calculated as 0.3 %, 0.4 %, 1.3 % for BHA-1 $BaZrO_3$, 0.6 %, 1.5 %, and 2.7 % for BHA-3 $BaZrO_3$, and 1.9 %, 3.7 %, and 10.7 % for BHA-5 $BaZrO_3$ composites. It is seen that the addition of $BaZrO_3$ to BHA causes a decrease in the HA percentage up to 89.3. However, the percentage of HA in BHA-TiO_2 [60] and BHA-ZrO_2 [61] composites were calculated as 49 %, and 22.6 %, respectively. This means that adding $BaZrO_3$ to BHA contributes to a decrease in the decomposition rate of BHA.

HA is thermally unstable between 1100 and 1400 °C in the HA-ZrO_2 system, and it decomposes into β- and α-TCP, and CaO. Moreover, the CaO in this system reacts with ZrO_2 to form $CaZrO_3$ [62], according to Reaction 1 [63].

$$Ca_{10}(PO_4)_6(OH)_2 + ZrO_2 \rightarrow 3Ca_3(PO_4)_2 + CaZrO_3 + H_2O \quad (1)$$

The $CaZrO_3$ formed in the HA-ZrO_2 system has also been detected in the $BaZrO_3$-added BHAs. However, $BaZrO_3$ added BHAs decomposed to TTCP instead of β- and α-TCP. HA decomposes between 700 and 1400 °C as shown in Reactions 2, and 3 [64], depending on the atmosphere of the sintering, the stoichiometric composition, and other factors [65].

$$Ca_{10}(PO_4)_6(OH)_2 \rightarrow 3Ca_3(PO_4)_2 + CaO + H_2O \quad (2)$$

$$3Ca_3(PO_4)_2 + CaO \rightarrow Ca_4O(PO_4)_2 \quad (3)$$

The TTCP formation in the BHA-1 % $BaZrO_3$ composite is due to the reaction of β- and α-TCP with CaO, as seen in Reaction 3. The formation of TTCP in the BHA-3$BaZrO_3$ and BHA-5$BaZrO_3$ composites can be explained by Reaction 4.

$$Ca_{10}(PO_4)_6(OH)_2 + 7BaZrO_3 \rightarrow Ba_2ZrO_4 + \text{Sigma-}Ba_2P_2O_7 + Ba_3P_2O_8 + 6CaZrO_3 + Ca_4O(PO_4)_2 + H_2O \quad (4)$$

It was concluded that this could be due to three reasons: First is the formation of $CaZrO_3$ as seen in Reaction 1. The second is due to the reaction of β- and α-TCP with CaO, as in the BHA-1$BaZrO_3$ composite. The third is the formation of the Sigma-$Ba_2P_2O_7$ and $Ba_3P_2O_8$ phases due to the diffusion of phosphorus (ion radius: 0.38 Å [66]) into the Ba-O (2.948 Å [67]) gap. It has been concluded that these phases prevent the formation of TCPs, in a free form. The same effect of phosphorus ions has also been confirmed for HA-Ti composites [68].

Figure 3 shows the average grain sizes and surface morphologies of the samples sintered between 1100 and 1300 ºC. The average grain size of pure BHA increased from 0.653 ± 0.029 μ to 2.838 ± 0.322 μ. It is in good agreement with Ref [69]. Although the BHA decomposed into β- and α-TCP just like at 1200 °C, its sintering at 1300 °C caused microcracking. We concluded that it might be related to various reasons: the BHA sintered at 1200 °C contains a porosity of 12.49 ± 1.50 % (Table 2), and the presence of up to 10 % porosity in HAs facilitates the removal of unstable OH^- without microcracking [44]. Microcracking occurs when a certain critical grain size is exceeded and the densification is higher than 90 % [70]. The necessary grain size and the densification rates have been calculated as 1.5 μm and 98 % for Ref [71], and as 0.4 μm and 99.5 % for Ref [72], respectively. It was observed that the average grain size of BHA-$BaZrO_3$ composites sintered at 1200 and 1300 °C was lower than that of pure BHA. It is thought that this is related to the intermediate phases, namely: Ba_2ZrO_4, sigma-BaP_2O_7, $Ba_3P_2O_8$ and $CaZrO_3$, formed between the BHA and $BaZrO_3$ particulates. As stated in Ref [73], Ba_2ZrO_4 inhibits the grain growth in $BaZrO_3$ doped ceramics. Studies on barium-substituted hydroxyapatites (Ba-HAs) [74-76] have reported that sigma-BaP_2O_7 and $Ba_3P_2O_8$ phases contribute to a grain size reduction in the HA matrix material. $CaZrO_3$ is located at the grain boundary of HA grains and acts as an effective grain growth inhibitor to the HAp grains [77]. These phases failed to show this behaviour in the BHA-5$BaZrO_3$ composite because the addition of $BaZrO_3$ at an amount of 5 wt. % causes a decrease in BHA's sintering behaviour. The average grain size of BHA- 5 wt. % $BaZrO_3$ composite of 0.845 ± 0.043 μ at 1100 °C increased to 1.573 ± ± 0.037 μ at 1300 ºC. However, the BHA-5 wt. % $BaZrO_3$ composite sintered at 1300 °C consists of pores located at the grain boundaries. The same microstructure was also confirmed for BHAs doped with 5 wt. % of –SiO_2, –MgO, –Al_2O_3 and –ZrO_2 [78], but microcracking was noted on the surface of these composites. The key factor associated with microcracking in these composites is the greater mismatch of thermal expansion coefficients (TECs) between the HA and dopant materials (HA: 12 $\times 10^{-6}$ ºC [79], SiO_2: 5.8 $\times 10^{-6}$ ºC [80], MgO: 6.5 $\times 10^{-6}$ ºC [81], Al_2O_3: 8.0 $\times 10^{-6}$ ºC [82], % 3 Ytrria Stabilised-ZrO_2: 5.5 $\times 10^{-6}$ ºC [83], $BaZrO_3$: 8.7 $\times 10^{-6}$ ºC [34]).

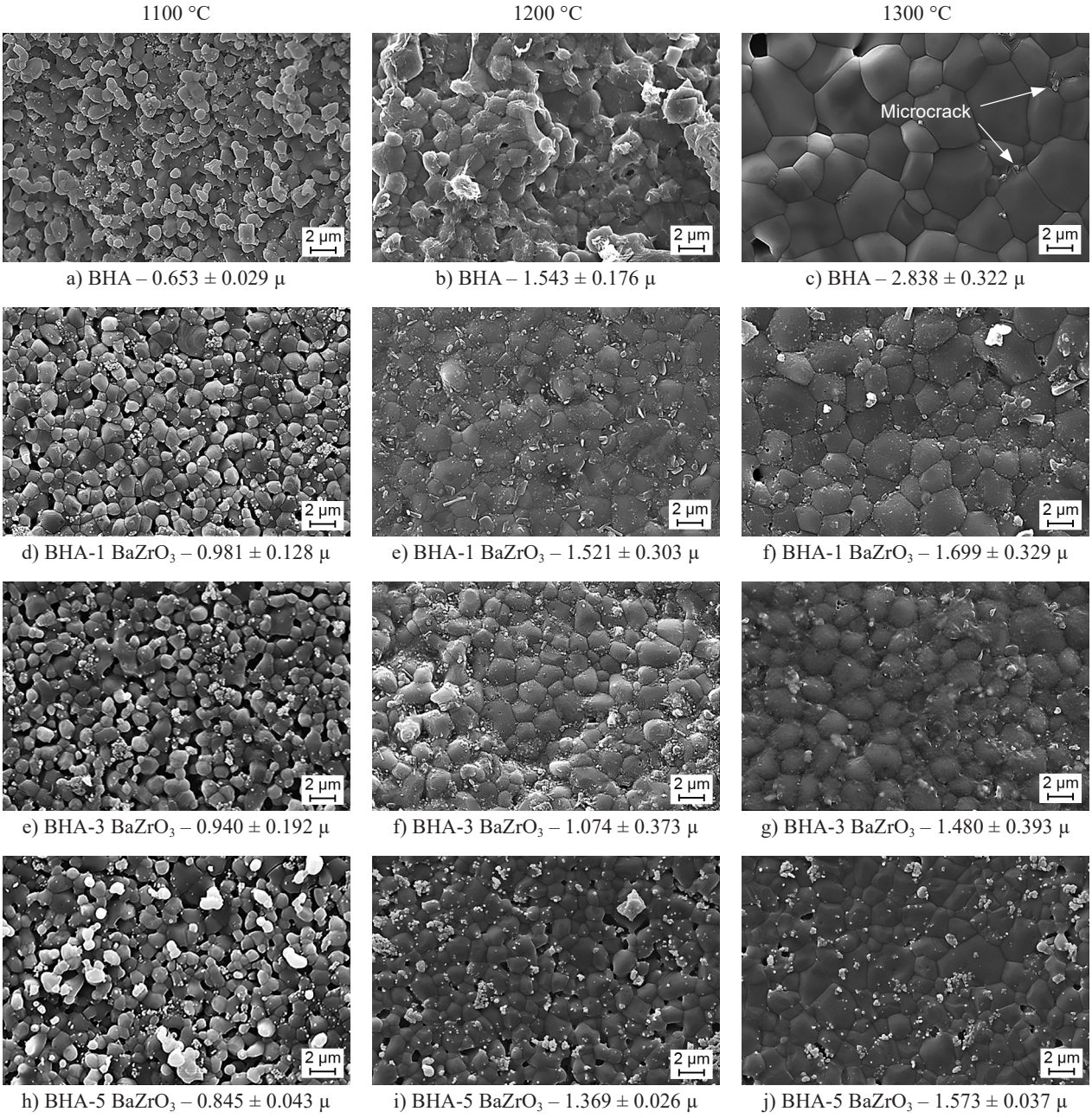

a) BHA – 0.653 ± 0.029 µ
b) BHA – 1.543 ± 0.176 µ
c) BHA – 2.838 ± 0.322 µ
d) BHA-1 $BaZrO_3$ – 0.981 ± 0.128 µ
e) BHA-1 $BaZrO_3$ – 1.521 ± 0.303 µ
f) BHA-1 $BaZrO_3$ – 1.699 ± 0.329 µ
e) BHA-3 $BaZrO_3$ – 0.940 ± 0.192 µ
f) BHA-3 $BaZrO_3$ – 1.074 ± 0.373 µ
g) BHA-3 $BaZrO_3$ – 1.480 ± 0.393 µ
h) BHA-5 $BaZrO_3$ – 0.845 ± 0.043 µ
i) BHA-5 $BaZrO_3$ – 1.369 ± 0.026 µ
j) BHA-5 $BaZrO_3$ – 1.573 ± 0.037 µ

Figure 3. The average grain size and surface morphologies of the samples sintered between 1100 and 1300 °C.

The physical, and mechanical properties of BHA with and without $BaZrO_3$ additives are tabulated in Table 2. In the samples sintered up to 1100 °C, a maximum shrinkage of about 6 % was observed. After a sharp increase in shrinkage at 1200 °C, the shrinkage of BHA without $BaZrO_3$ reached a maximum of 12.02 ± 0.52 %, and it reached to 12.34 ± 0.53 % for the $BaZrO_3$ added samples at 1300 °C. As stated by Ref [84], BHA milled at 400 rpm for 16 h and then pelleted at 130 MPa exhibited a shrinkage of about 15 % when it was sintered at 1300 °C. There are two reasons for the lower shrinkage of BHA when compared with this study. First, it is the smaller particles that fill the voids between the larger ones resulting in higher green densities. The higher green density leads to the higher shrinkage [85]. Second, the lowest shrinkage value occurred at the highest uniaxial pressure because the density between the powders was perfect in the green bodies, so the sintering process did not require high shrinkage to form grain bonds in the sintered bodies [86]. The shrinkage behaviour of HA-based composites is affected by the differential shrinkage behaviour of the various component phases that occurs between the HA and dopant materials [87]. It is seen that the $BaZrO_3$ added samples showed higher shrinkage than the pure BHA, when sintering was carried out between 900 and 1100 °C. We considered that it is related to the

growing of the $BaZrO_3$ particulates and where they are located which fills the pores between the BHA particles without reacting. This is due to the thermal expansion coefficient of $BaZrO_3$ being lower than that of HA. As the sintering temperature was increased from 1100 °C to 1300 °C, the shrinkage rates of the composites decreased with an increasing $BaZrO_3$ ratio. That is related to three reasons: Firstly, the loss of OH enhances the formation of $CaZrO_3$ and the formation of $CaZrO_3$ is accompanied by a volume expansion; the resulting sintering shrinkage is, therefore, small [77]. Secondly, the increase in the decomposition rate of BHA with an increasing $BaZrO_3$ ratio. Thirdly, the necessity for a temperature as high as 1600 °C [88] to obtain more shrinkage by increasing the $BaZrO_3$ ratio. The density of the BHA-5$BaZrO_3$ composite increased from 2.09 ± 0.01 g·cm^{-3} at 900 °C to 2.89 ± 0.02 g·cm^{-3} at 1300 °C. It is seen that the density of the BHA-5$BaZrO_3$ composite at 1300 °C is slightly higher than the pure BHA. The same regime, at all the sintering temperatures, was also observed in other composites. It is thought that this is related to the phases formed at the interfaces between the BHA and $BaZrO_3$ particulates that have a higher theoretical density than HA (Ba_2ZrO_4: 5.94 g·cm^{-3} [89], σ-$Ba_2P_2O_7$: 4.11 g·cm^{-3}, $Ba_3P_2O_8$: 5.26 g·cm^{-3} [90], $CaZrO_3$: 4.78 g·cm^{-3} [91], TTCP: 3.05 g·cm^{-3} [92], β-TCP: 3.07 g·cm^{-3} [93], and

Table 2. Physical, and mechanical properties of the BHA with and without $BaZrO_3$ additives as a function of the sintering temperature.

Temp. (°C)	Property	Pure BHA	BHA-1 $BaZrO_3$	BHA-3 $BaZrO_3$	BHA-5 $BaZrO_3$
900	Shrinkage (%)	0.74 ± 0.37	1.584 ± 0.86	1.581 ± 0.73	1.04 ± 0.36
1000		1.21 ± 0.53	2.68 ± 0.92	2.30 ± 0.86	1.45 ± 0.36
1100		4.57 ± 0.94	6.18 ± 0.99	3.61 ± 0.54	3.40 ± 0.45
1200		10.22 ± 0.31	10.92 ± 1.26	8.88 ± 0.37	7.91 ± 0.39
1300		12.02 ± 0.52	12.34 ± 0.53	12.29 ± 0.23	12.03 ± 0.65
900	Density (g·cm^{-3})	2.03 ± 0.02	2.094 ± 0.00	2.092 ± 0.00	2.04 ± 0.02
1000		2.05 ± 0.03	2.13 ± 0.01	2.097 ± 0.00	2.09 ± 0.01
1100		2.24 ± 0.00	2.33 ± 0.00	2.26 ± 0.01	2.22 ± 0.01
1200		2.70 ± 0.03	2.68 ± 0.00	2.66 ± 0.02	2.53 ± 0.03
1300		2.86 ± 0.04	2.94 ± 0.02	2.96 ± 0.00	2.89 ± 0.02
900	Relative density (%)	64.55 ± 0.69	65.98 ± 0.28	65.38 ± 0.23	63.29 ± 0.74
1000		65.16 ± 0.95	67.47 ± 0.53	65.47 ± 0.15	64.76 ± 0.42
1100		71.24 ± 0.31	73.62 ± 0.01	70.81 ± 0.34	68.74 ± 0.36
1200		85.74 ± 1.03	79.68 ± 1.93	83.12 ± 0.72	78.37 ± 1.10
1300		90.77 ± 1.51	92.91 ± 0.68	92.62 ± 0.06	89.51 ± 0.90
900	Porosity (%)	34.96 ± 0.56	31.84 ± 1.16	33.28 ± 3.60	36.70 ± 0.74
1000		34.32 ± 0.86	30.55 ± 2.63	30.95 ± 0.63	35.23 ± 0.42
1100		28.49 ± 0.41	26.20 ± 0.29	28.06 ± 0.56	31.25 ± 0.36
1200		12.49 ± 1.50	14.71 ± 1.21	14.62 ± 0.11	21.62 ± 1.10
1300		1.12 ± 0.75	1.50 ± 0.83	1.01 ± 0.20	1.48 ± 0.90
900	Hardness (GPa)	0.45 ± 0.04	0.53 ± 0.08	0.58 ± 0.07	0.49 ± 0.09
1000		0.50 ± 0.08	0.66 ± 0.10	0.64 ± 0.07	0.58 ± 0.07
1100		1.37 ± 0.11	1.45 ± 0.16	1.44 ± 0.16	1.38 ± 0.12
1200		2.89 ± 0.27	2.98 ± 0.20	3.18 ± 0.19	2.64 ± 0.24
1300		4.19 ± 0.31	4.33 ± 0.60	4.41 ± 0.25	4.22 ± 0.31
900	Fracture toughness (MPa·m$^{1/2}$)	0.30 ± 0.03	0.48 ± 0.04	0.50 ± 0.03	0.33 ± 0.01
1000		0.32 ± 0.04	0.56 ± 0.06	0.53 ± 0.04	0.38 ± 0.03
1100		0.74 ± 0.05	0.83 ± 0.09	0.79 ± 0.07	0.70 ± 0.06
1200		0.85 ± 0.02	1.22 ± 0.11	1.56 ± 0.09	0.78 ± 0.07
1300		0.99 ± 0.13	1.40 ± 0.15	1.80 ± 0.12	1.02 ± 0.10
900	Brittleness index (μ$^{-1/2}$)	1.51 ± 0.15	1.10 ± 0.02	1.16 ± 0.01	1.48 ± 0.04
1000		1.56 ± 0.25	1.17 ± 0.05	1.20 ± 0.02	1.52 ± 0.07
1100		1.85 ± 0.15	1.74 ± 0.09	1.82 ± 0.11	1.97 ± 0.10
1200		3.40 ± 0.32	2.44 ± 0.10	1.89 ± 0.14	3.38 ± 0.15
1300		4.24 ± 0.31	3.09 ± 0.12	2.45 ± 0.15	4.13 ± 0.18
900	Compressive strength (%)	29.25 ± 4.27	36.66 ± 9.07	31.00 ± 9.01	30.66 ± 5.29
1000		32.50 ± 8.50	43.33 ± 5.50	42.00 ± 3.60	38.66 ± 13.86
1100		59.75 ± 5.31	99.33 ± 7.23	80.66 ± 5.85	52.00 ± 4.24
1200		108.20 ± 6.45	111.66 ± 9.29	145.33 ± 3.21	101.66 ± 10.69
1300		115.75 ± 4.27	156.00 ± 11.93	173.66 ± 13.61	127.66 ± 5.65

α-TCP: 2.86 g·cm^{-3} [94]). Although the densities of the pure BHA and composites increased with an increasing sintering temperature, they could not reach the theoretical values calculated in the experimental section, which is due to the porosity. The samples sintered up to 1100 °C showed a slight decrease in porosity from 36.70 ± 0.74 % to 26.20 ± 0.29 % due to the local interconnections between the grains. Sintering at 1200 °C contributed to the reduction of porosity up to 12 % and to the positioning of the porosities between the BHA-BHA and BHA-$BaZrO_3$ particulates. The porosity of the samples showed a sharp decrease from 12 % to 1-1.5 % when sintering was carried out at 1300 °C. The porosity of 1-1.5 % obtained from the composites are lower than that of the TiO_2 (7 %) and Al_2O_3 (18 %)-doped HAs [95]. This is related to the increase in the decomposition rate of HA when it is doped with TiO_2 and Al_2O_3. Dense HA bioceramics are used for implant-coating targets or bone repair, and fillers are typically prepared using high-temperature sintering processes. It has been reported that the sintering temperature affects the porosity, grain size, densification, shrinkage, calcium/phosphorus (Ca/P) ratio, and content of the amorphous phase, which can alter the mechanical and biological properties of the resulting CaP bioceramics. In dense bioceramics, mechanical properties can significantly improve with a decreasing porosity and grain size [95]. As the sintering temperature increased from 900 °C to 1300 °C, the relative density of the samples increased. The highest relative density of BHA was calculated as 90.77 ± 1.51 %. It changes between 89.51 ± 0.90 % and 92.62 ± 0.06 % for the composites. While HA ceramics can be sintered at a high relative density by pressureless sintering in the temperature range of 1100-1300 °C, it is not possible to reach a high relative density in the above temperature range for various reasons in most HA-based composites: The first reason is the making of HA composites with reinforcing reagents and dopant materials causes an increase in the decomposition rate of the HA. Secondly, the intermediate phases formed as a result of the reactions between the additives and HA cause a decrease in the sintering ability of the system, as in HA-B_2O_3 [96], and HA-TiO_2 [97]. The hardness of 0.45 ± 0.04 GPa, and compressive strength of 29.25 MPa of pure BHA at 900 °C increased with an increasing sintering temperature and reached 4.19 GPa ± 0.31 GPa, and 115.75 ± 4.27 MPa at 1300 °C, respectively. Although BHA is composed of β and α-TCPs, as shown in Figure 1, its hardness and compressive strength were higher than in previous studies [15-17]. The reason is that the BHA powders in these studies have a starting grain size of 300 µ. Previous studies [98, 99] show that the hardness, fracture toughness and compressive strength of HA ceramics increase with a decrease in the starting grain size. The presence of β- and α-TCPs in the HA in a small amount is useful to where it can improve the bioactive and bioresorbable properties of the HA. However, the excess amount of β- and α-TCPs in the HA causes a decrease in the mechanical strength of HA-based bioceramics [100]. It is reported that if a reinforcing agent, such as alumina, titania, and zirconia, is added to HA, the mechanical properties are reduced since the decomposition rate of HA is up to 70 %, and the samples are very brittle and friable [101]. The hardness of $BaZrO_3$ added BHAs increased with an increasing sintering temperature as in the pure BHA. A maximum hardness of 4.41 ± 0.60 GPa was obtained for the composites. It meets the minimum hardness of 4.2 GPa [102] for cortical bone applications. The highest hardness values of the composites are higher than that of pure BHA for various reasons: the hardness increase with a decreasing grain size is typically attributed to the reduced free path for dislocations in both metals and ceramics [103]. The polyphase HAs partially decomposed to TTCP exhibit greater hardness than monophase HAs [104]. Although the amount of the TTCP phase after sintering at 1300 °C in the BHA-5 $BaZrO_3$ composite is higher than that of BHA-1 $BaZrO_3$ and BHA-3 $BaZrO_3$ composites, there are two reasons for its low hardness value: Firstly, the relative density value of BHA-5$BaZrO_3$ composite is lower than the others. Secondly, obtaining a more heterogeneous microstructure compared to the other composites. The fracture toughness is defined as the resistance offered by a material to the sudden propagation of a crack [105]. The highest fracture toughness of HA ceramics changes between 0.6-1.25 MPa·m$^{1/2}$ depending on the grain size [106], powder morphology [107], sintering method [108], and sintering atmosphere [109]. However, it de-creases when the relative density of HA exceeds ≈ 95 % [110] due to an increase in grain size. The fracture tough-ness of BHA without $BaZrO_3$ increased to the highest value of 0.99 ± 0.13 MPa·m$^{1/2}$ when sintering was performed at 1300 °C. It was significantly improved by adding 1 wt. % and 3 wt. % of $BaZrO_3$, and it attained 1.40 ± 0.15 and 1.80 ± 0.12 MPa·m$^{1/2}$ with an increase of 41 % and 81 %, respectively. The mechanisms that increase the toughness of the composites compared to BHA involve an expansion of the energy required to extend a crack since there are other crystalline phases that are widely spread in the microstructure detected by the XRD analysis. As happens with other ceramic matrix composites, a combination of crack bridging, crack de-flection, and microcracking occurs with a great reflection in the fracture toughness improvement [31]. The latter mechanism may appear as a consequence of the properties mismatched between the adjacent grains and by the phase transformation. The presence of tougher phases in a composite, besides causing some crack in-flection, can also be responsible for some crack bifur-cation around the grains leading to crack bridging. Transformation-toughened ceramics owe their high toughness to the stress-induced transformation of a meta-stable phase in the vicinity of a propagating crack. The transformation of HA to TTCP acts as a

barrier to the propagation of the cracks during the indentation test [111]. The fracture toughness of the BHA-3 $BaZrO_3$ composite is higher than that of HA-MnO_2 (1.65 MPa·$m^{1/2}$ [112]) and HA-MgO (1.78 MPa·$m^{1/2}$ [113]) composites. It is lower than cortical bone (2-6 MPa·$m^{1/2}$ [114]), so its use as a load-bearing material in the human body should be avoided [115]. The brittle index of pure BHA reached the maximum value of 4.24 ± 0.31 $\mu^{-1/2}$ by increasing sintering temperature, which was calculated as 4.6 $\mu^{-1/2}$ [116], 4.85 $\mu^{-1/2}$ [117], 9.39 $\mu^{-1/2}$ [118], 24.8 $\mu^{-1/2}$ [46], 25.6 $\mu^{-1/2}$ [119]. As the brittleness index increases, the brittleness of the material increases. This means that BHA used as a matrix material in the present study has lower brittleness than the previous studies. The brittle-ness index of $BaZrO_3$ added BHAs changes between 1.10 ± 0.02 and 4.13 ± 0.18 $\mu^{-1/2}$. A reduction of about 42 % in the brittleness index of BHA was achieved by the addition of $BaZrO_3$ at an amount of 3 wt. %, when sintering was performed at 1300 °C. It has also been observed that the brittleness index of the BHA-3 $BaZrO_3$ composite is lower than that of HA-3 wt. % MgO (3.72 $\mu m^{-1/2}$ [120]) and HA-3 wt. % Al_2O_3 (4.28 $\mu m^{-1/2}$ [121]) composites. The highest compression strength of BHA reached 173.66 ± ± 13.61 MPa with an increase of 50 %, by the addition of $BaZrO_3$ at amount of 3 wt. %. This is related to two reasons: Firstly, the high young modulus of $BaZrO_3$ (E = 125 GPa [122]) and $CaZrO_3$ (E = 228 GPa [123])

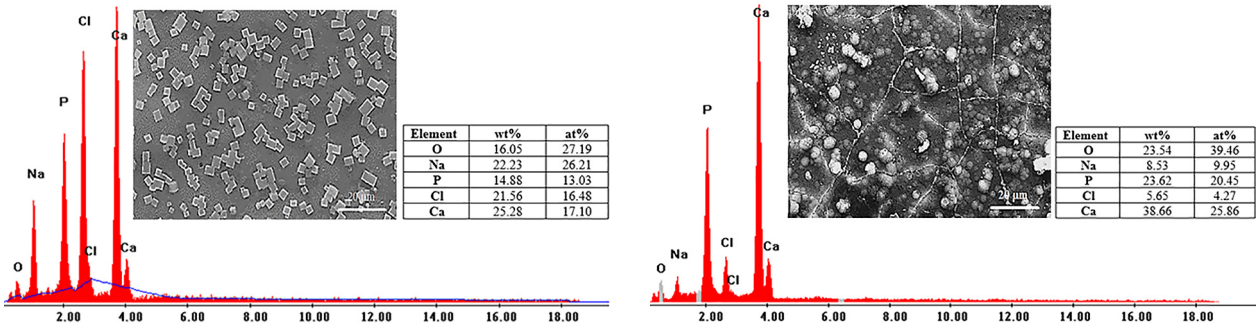

a) BHA – 14 days b) BHA – 28 days

Figure 4. Surface morphology of the pure BHA subjected to *in vitro* bioactivity testing for 14 and 28 days.

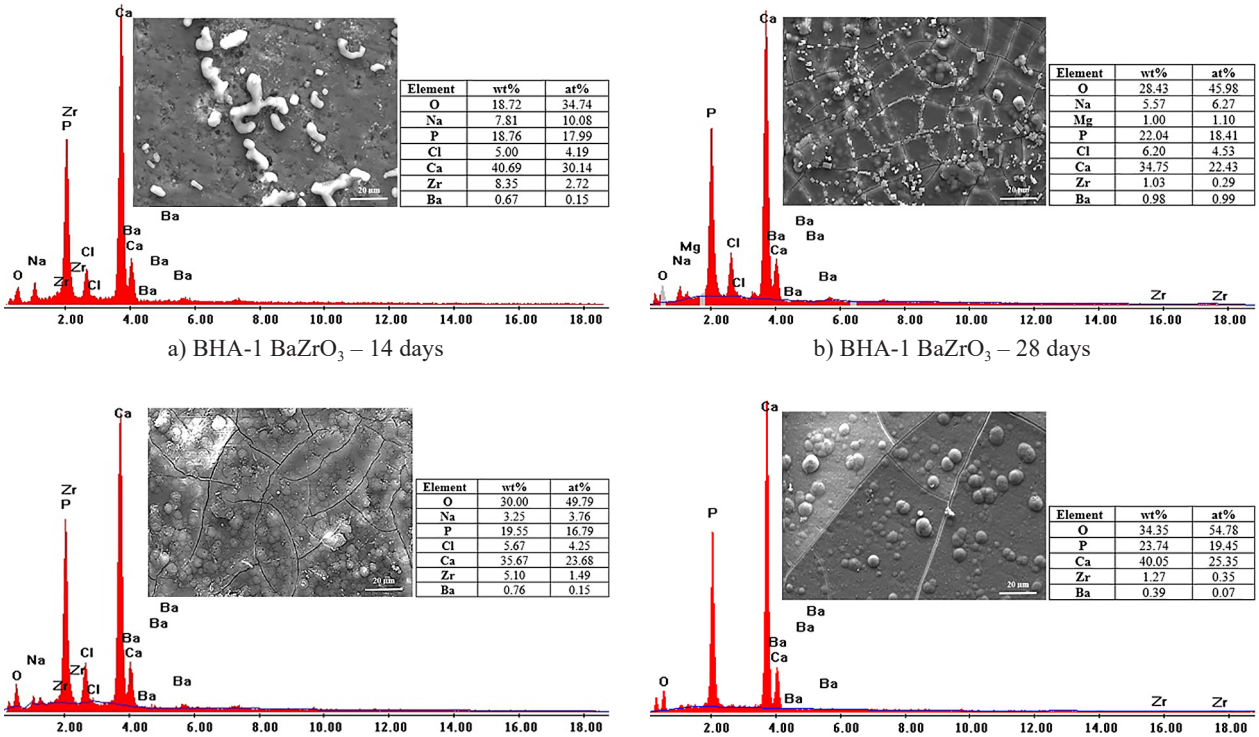

a) BHA-1 $BaZrO_3$ – 14 days b) BHA-1 $BaZrO_3$ – 28 days

c) BHA-3 $BaZrO_3$ – 14 days d) BHA-3 $BaZrO_3$ – 28 days

Figure 5. Surface morphologies of the BHA-1 $BaZrO_3$ and BHA-3B aZrO_3 composites subjected to *in vitro* bioactivity testing for 14 and 28 days.

promotes the reinforcement of the HA matrix (E = = ~95 GPa), and consequently improve the resistance [124]. Secondly, the Sigma-$Ba_2P_2O_7$ and $Ba_3P_2O_8$ phases contribute to the densification. Increasing the densification leads to a decrease in the porosity, which causes a decrease in the cross-sectional area on which the load is applied [125]. Simulated body fluid (SBF) is a metastable calcium phosphate solution that is supersaturated relative to apatite. It can be used to study the ability of materials to induce bone-like apatite and to reflect the biological activity of materials [126].

Figure 4 shows the surface morphology of the pure BHA subjected to *in vitro* bioactivity testing for 14 and 28 days. BHA has a chemical composition similar to human bone, with trace amounts of carbonate, sodium, magnesium, iron, fluoride, silicate, and chloride [127]. It is seen that the apatite layer on the surface of BHA increases with an increase in the SBF time. Although many apatites in a cubic form were imaged after 14 days of immersion on the surface of pure BHA, its surface was covered by an apatite layer when immersion time is reached 28 days. The Ca/P ratio in pure BHA was calculated as 1.69 and 1.63, which are close to the Ca/P ratio for hydroxyapatite (1.67) [128], respectively, at 14 and 28 days.

Figure 5 shows the surface morphologies of BHA-1 $BaZrO_3$ and BHA-3 $BaZrO_3$ composites subjected to *in vitro* bioactivity testing for 14 and 28 days. As a result of 14 days of immersion, although a low-rate apatite structure was formed in BHA-1 $BaZrO_3$, the whole surface of the BHA-3 $BaZrO_3$ composite was covered with apatite. At this immersion time, the Ca/P ratio for BHA-1$BaZrO_3$ is 2.16 and for BHA-3 $BaZrO_3$ is 1.82. When the immersion time reached 28 days, the surfaces of the BHA-$BaZrO_3$ composites were covered entirely with apatite as in BHA. The Ca/P ratios were measured as 1.57 for BHA-1 $BaZrO_3$ and 1.68 for BHA-3 $BaZrO_3$. The crack-like regions that formed along the interfaces of the apatite layers on the surface of the samples are drying cracks [129].

In vitro bioactivity studies showed that the addition of $BaZrO_3$ at an amount of 3 wt. % to BHA greatly increased the bioactivity of the BHA. There are several reasons for this. Firstly, the presence of $CaZrO_3$ contributes to an increase in the bioactivity of HA [130]. Secondly, the low grain size of BHA-3 $BaZrO_3$ compared to the pure BHA and BHA-1 $BaZrO_3$ composite. It has been confirmed in previous studies [131,132] that a decrease in grain size increases the *in vitro* bioactivity of HA based bioceramics.

CONCLUSIONS

In the present study, the potential of $BaZrO_3$ on the sintering performance and properties of BHA was evaluated by microstructural and mechanical analyses. While BHA without $BaZrO_3$ started to decompose to β-TCP at a rate of 3.3 % at 1100 °C, it decomposed into β- and α-TCP phases at a total rate of 4.7 % when it was sintered at 1300 °C. $BaZrO_3$ added BHAs consist of the phases that are HA, $BaZrO_3$, Ba_2ZrO_4, Sigma-$Ba_2P_2O_7$, $Ba_3P_2O_8$, and $CaZrO_3$. TTCP was detected as the decomposition phase in the $BaZrO_3$ composites. An increase in the $BaZrO_3$ ratio led to an increase in the amount of TTCP, and it was calculated as 10.7 % after sintering at 1300 °C. The addition of the $BaZrO_3$ at amount of 3 wt. % was determined to have the potential to improve the sinterability and properties of BHA. It increased the fracture toughness from 0.99 ± 0.13 to 1.80 ± 0.12 MPa·$m^{1/2}$, and the compression strength from 115.75 ± 4.27 to 173.66 ± 13.61 MPa, but it decreased the brittleness index from 4.24 ± 0.31 to 2.45 ± 0.15 $\mu^{-1/2}$. It also contributed to greatly increasing the bioactivity of the BHA. However; the BHA-3 wt. % $BaZrO_3$ composite should be avoided for use in load bearing applications in the human body due to its insufficient fracture toughness.

REFERENCES

1. Khamkongkaeo A., Boonchuduang T., Klysubun, W., Amonpattaratkit P., Chunate H., Tuchinda N., Pimsawat A., Daengsakul S., Suksangrat P., Sailuam W., Vongpramate D., Bootchanont A., Lohwongwatan B. (2021): Sintering behavior and mechanical properties of hydroxyapatite ceramics prepared from Nile Tilapia (Oreochromis niloticus) bone and commercial powder for biomedical applications. *Ceramics International*, *47*, 34575-34584. doi: 10.1016/j.ceramint.2021.08.372
2. Zhao X., Yang Z., Wang W., Jiang G., Wei S., Liu A., Guan J., Wang P. (2022): Preparation of carbon fiber/Mg-doped nano-hydroxyapatite composites under low temperature by pressureless sintering. *Ceramics International*, *48*, 674-683. doi: 10.1016/j.ceramint.2021.09.147
3. Mohd Pu'ad N.A.S., Koshy P., Abdullah H.Z., Idris M.I., Lee T.C. (2019): Syntheses of hydroxyapatite from natural sources. *Heliyon*, *5*[5], e01588. doi: 10.1016/j.heliyon.2019.e01588
4. Nasker P., Samanta A., Rudra S., Sinha A., Mukhopadhyay A.K., Das M. (2019): Effect of fluorine substitution on sintering behaviour, mechanical and bioactivity of hydroxyapatite. *Journal of the Mechanical Behavior of Biomedical Materials*, *95*, 136-142. doi: 10.1016/j.jmbbm.2019.03.032
5. Ali M.M.S., Imam D.M., ElNad Y.A. (2021): Vanadium (V) removal and recovery by adsorption onto modifed activated carbon derived from natural hydroxyapatite. *Journal of the Iranian Chemical Society*, *18*, 2771-2784. doi: 10.1007/s13738-021-02227-7
6. Rajesh R., Hariharasubramanian A., Ravichandran Y.D. (2012): Chicken bone as a bioresource for the bioceramic (hydroxyapatite). *Phosphorus, Sulfur, and Silicon and the Related Elements*, *187*, 914-925. doi: 10.1080/10426507.2011.650806
7. Akyurt N., Yetmez M., Oktar, F.N. (2019): Studies on goat hydroxyapatite/commercial inert glass biocomposites. *Journal of the Australian Ceramic Society*, *55*, 697-702. doi: 10.1007/s41779-018-0279-z

8. Sobczak-Kupiec A., Wzorek Z., Kijkowska R., Kowalski Z. (2013): Effect of calcination conditions of pork bone sludge on behaviour of hydroxyapatite in simulated body fluid. *Bulletin of Materials Science*, *36* [4], 755-764. doi: 10.1007/s12034-013-0482-z
9. Demirkol N., Oktar F.N., Kayali E.S. (2012): Mechanical and Microstructural properties of sheep hydroxyapatite (SHA)-niobium oxide composites. *Acta Physica Polonica A*, *121*[1], 274-276. doi: 10.12693/APhysPolA.121.274
10. Ayatollahi M.R., Yahya M.Y., Shirazi H.A., Hassan S.A. (2015): Mechanical and tribological properties of hydroxyapatite nanoparticles extracted from natural bovine bone and the bone cement developed by nano-sized bovine hydroxyapatite filler. *Ceramics International*, *41*, 10818-10827. doi: 10.1016/j.ceramint.2015.05.021
11. López A.M., del Pozo P.P., Muela C.M., Caicoya S.O., Cuéllar C.N., Escobar J.I.S. (2015): Maxillary sinus augmentation with bovine hydroxyapatite alone: A safe technique with predictable outcomes in patients with severe maxillary atrophy. *Revista Española de Cirugía Oral y Maxilofacial*, *37*[2], 87-92. doi: 10.1016/j.maxilo.2014.07.010
12. Nam J.W., Khureltogtokh S., Choi H.M., Lee A.R., Park Y.B., Kim H.J. (2017): Randomised controlled clinical trial of augmentation of the alveolar ridge using recombinant human bone morphogenetic protein 2 with hydroxyapatite and bovine-derived xenografts: comparison of changes in volume. *British Journal of Oral and Maxillofacial Surgery*, *55*, 822-829. doi: 10.1016/j.bjoms.2017.07.017
13. Odusote J.K., Danyuo Y., Baruwa A.D., Azeez A.A. (2019): Synthesis and characterization of hydroxyapatite from bovine bone for production of dental implant. *Journal of Applied Biomaterials & Functional Materials*, *17*[2], doi: 10.1177/2280800019836829
14. Niakan A., Ramesh S., Hamdi M., Jahanshahi A., Tan C.Y., Ching Y.C., Tolouei R. (2014): Thermal treatment and properties of bovine hydroxyapatite. *Materials Research Innovations*, *18*[6], 117-120. doi: 10.1179/1432891714Z.000000000941
15. Goller G., Oktar F.N., Agathopoulos S., Tulyaganov D.U., Ferreira J.M.F., Kayali E.S., Peker I. (2006): The influence of sintering temperature on mechanical and microstructural properties of bovine hydroxyapatite. *Journal of Sol-Gel Science and Technology*, *37*, 111-115. doi: 10.1007/s10971-006-6428-9
16. Gören Ş., Gökbayrak H., Altintaş S. (2004): Production of hydroxylapatite from animal bone. *Key Engineering Materials*, *264-268*[III], 1949-1952. doi: 10.4028/www.scientific.net/KEM.264-268.1949
17. Oktar F.N., Aydin H., Goller G., Agathopoulos S., Rocha G., Sennaroglu B., Kayali S. (2006): Influence of sintering temperature on mechanical properties of biologically derived hydroxyapatite bodies. *Key Engineering Materials*, *309-311*, 45-48. doi: 10.4028/www.scientific.net/KEM.309-311.45
18. Oktar F.N., Meydanoglu O., Goller G., Agathopoulos S., Rocha G., Ozyegin S., Eruslu N., Peker I., Kayali S. (2006): Sintering effects on mechanical properties of hydroxyapatite-titanium dioxide (HA-TiO_2) composites. *Key Engineering Materials*, *309-311*, 355-358. doi: 10.4028/www.scientific.net/KEM.309-311.355
19. Gunduz O., Gode C., Ahmad Z., Gökçe H., Yetmez M., Kalkandelen C., Sahin Y.M., Oktar F.N. (2014): Preparation and evaluation of cerium oxide-bovine hydroxyapatite composites for biomedical engineering applications. *Journal of the Mechanical Behavior of Biomedical Materials*, *35*, 70-76. doi: 10.1016/j.jmbbm.2014.03.004
20. Oktar F.N., Demirer M.R., Gunduz O., Genc Y., Agathopoulos S., Peker I., Ozyegin L.S., Salman S. (2006): Sintering effect on mechanical properties of composites of bovine hydroxyapatite (BHA) and Li_2O. *Key Engineering Materials*, *309-311*, 49-52. doi: 10.4028/www.scientific.net/KEM.309-311.49
21. Tecu C., Antoniac I., Goller G., Yavas B., Gheorghe D., Antonıac A., Cıuca I., Semenescu A., Raiciu A.D., Cristescu I. (2019): The sintering behaviour and mechanical properties of hydroxyapatite- based composites for bone tissue regeneration. *Materilae Plastice*, *56*[3], 644-648. doi: 10.37358/MP.19.3.5246
22. Oktar F.N., Ozyegin S., Meydanoglu O., Aydin H., Agathopoulos S., Rocha G., Sennaroglu B., Kayali S. (2006): Sintering effect on mechanical properties of composites of hydroxyapatite lanthanum oxide (HA-La_2O_3). *Key Engineering Materials*, *309-311*, 101-104. doi: 10.4028/www.scientific.net/KEM.309-311.101
23. Gunduz O., Daglılar S., Salman S., Ekren N., Agathopoulos S., Oktar F.N. (2008): Effect of yttria-doping on mechanical properties of bovine hydroxyapatite (BHA). *Journal of Composite Materials*, *42*, 1281-1287. doi: 10.1177/0021998308092196
24. Oktar F.N., Genc Y., Goller G., Agathopoulos S., Tulyaganov D.U., Ferreira J.M.F., Kayali E.S., Salman S. (2005): The influence of sintering temperature on the properties of composites of biologic hydroxyapatite and zirconia. *Key Engineering Materials*, *284-286*, 709-712. doi: 10.4028/www.scientific.net/KEM.284-286.709
25. Yetmez M., Erkmen Z.E., Kalkandelen C., Ficai A., Oktar F.N. (2017): Sintering effects of mullite-doping on mechanical properties of bovine hydroxyapatite. *Materials Science and Engineering C*, *77*, 470-475. doi: 10.1016/j.msec.2017.03.290
26. Catalgol Z. (2019): Sintering effect on borosilicate glass-bovine hydroxyapatite composites. *Journal of the Australian Ceramic Society*, *55*, 1075-1079. doi: 10.1007/s41779-019-00320-y
27. Gunduz O., Ozyegin L.S., Dorozhkin S., Meydanoglu O., Eruslu N., Kayali S., Goller G., Agathopoulos S., Oktar F.N. (2009): Bovine hydroxyapatite strontium oxide composites. *Key Engineering Materials*, *396-398*, 407-410. doi: 10.4028/www.scientific.net/KEM.396-398.407
28. Gunduz O., Ozyegin L.S., Dorozhkin S., Meydanoglu O., Eruslu N., Kayali S., Agathopoulos S., Oktar F.N. (2009): Bovine hydroxyapatite (BHA) boron oxide composites. *Key Engineering Materials*, *396-398*, 403-406. doi: 10.4028/www.scientific.net/KEM.396-398.403
29. Salman S., Oktar F.N., Gunduz O., Agathopoulos S., Öveçoğlu M.L., Kayalı E.S. (2007): Sintering effect on mechanical properties of composites made of bovine hydroxyapatite (BHA) and commercial inert glass (CIG). *Key Engineering Materials*, *330-332*, 189-192. doi: 10.4028/www.scientific.net/KEM.330-332.189
30. Ozturk S., Yetmez M. (2016): Studies on characterization of bovine hydroxyapatite/$CaTiO_3$ biocomposites. *Advances in Materials Science and Engineering*, doi: 10.1155/2016/6987218

31. Pazarlioglu S.S. (2022): The effect of alphalithium aluminate incorporation on the properties of bovine bone-derived hydroxyapatite. *Journal of the Australian Ceramic Society*, *58*, 1585-1601. doi: 10.1007/s41779-022-00796-1
32. Ramesh S., Natasha A.N., Tan C., Bang Y., Ramesh L.T., Ching S., Chandran C.Y. (2016): Direct conversion of eggshell to hydroxyapatite ceramic by a sintering method. *Ceramics International*, *42*, 78247829. doi: 10.1016/j.ceramint.2016.02.015
33. Andreja Z., Ressler A., Macan J. (2022): Perovskite oxides as active materials in novel alternatives to well-known technologies: A review. *Ceramics International*, *48*, 27240-27261. doi: 10.1016/j.ceramint.2022.06.152
34. Orak I., Karabulut A., Yiğit E., Sevgili Ö., Ruşen A., Ozel F. (2022): The diode and photodiode performances of $BaZrO_3$ perovskite-based device under the influence of thermal and light external stimuli. *Sensors and Actuators A: Physical*, *337*, 113413. doi: 10.1016/j.sna.2022.113413
35. Kayathiri C., Balu A.R., Suganya M., Vinitha G., Delcic Z., Balamurugan S., Karthika M., Anitha S., Prabavathi A. (2022): $BaZrO_3$ perovskite – A UV light mediated congo red dye deactivator catalyst with good optical switching and antimicrobial abilities green synthesized using Moringa oleifera leaf extract. *Materials Science and Engineering: B*, *278*, 115636. doi: 10.1016/j.mseb.2022.115636
36. Singh V., Watanabe S., Gundu Rao T.K., Lakshminarayana G. (2021): Structural, paramagnetic centres and luminescence investigations of the UV radiation-emitting $BaZrO_3$:Gd^{3+} perovskite ceramic prepared via sol-gel route. *Materials Science and Engineering: B*, *264*, 114971. doi: 10.1016/j.mseb.2020.114971
37. Wang L., Habibi M.H., Eldridge J.L., Guo S.M. (2014): Infrared radiactive properties of plasma-sprayed $BaZrO_3$ coatings. *Journal of the European Ceramic Society*, *34*[15], 3941-3949. doi: 10.1016/j.jeurceramsoc.2014.05.015
38. Shape Casting (2016): 6th International Symposium Edited by: M. Tiryakioğlu, M. Jolly, G. Byczynski, TMS (The Minerals, Metals & Materials Society)
39. Zhang L., Pu Y., Chen M. (2019): Influence of $BaZrO_3$ additive on the energy-storage properties of $0.775Na_{0.5}Bi_{0.5}TiO_{3-0.225}BaSnO_3$ relaxor ferroelectrics. *Journal of Alloys and Compounds*, *775*, 342-347. doi: 10.1016/j.jallcom.2018.10.025
40. Matsui M., Sakai N., Nariki S., Murakami M. (2001): Effect of ZrO_2, and $BaZrO_3$ addition on the microstructure and superconducting properties of melt processed $NdBa_2Cu_3O_{7-\delta}$. *Physica C Superconductivity*, *357-360*, 697-701. doi: 10.1016/S0921-4534(01)00320-3
41. Chakrapani V., Balkin D., Ginn P.M. (1993): The effects of second phase additions (SiC, $BaZrO_3$, $BaSnO_3$) on the microstructure and superconducting properties of zone melt textured $pBa_2Cu_3O_{7-x}$. *Applied Superconductivity*, *1*[1-2], 71-80. doi: 10.1016/0964-1807(93)90383-D
42. Zhou H., Maiorov B., Baily S.A., Dowden P.C., Kennison J.A., Stan L., Holesinger T.G., Jia Q.X., Foltynand S.R., Civale L. (2009): Thickness dependence of critical current density in $YBa_2Cu_3O_{7-\delta}$ films with $BaZrO_3$ and Y_2O_3 addition. *Superconductivity Science and Technology*, *22*, 085013. doi: 10.1088/0953-2048/22/8/085013
43. Zhang Y., Hao L., Savalani M.M., Harris R.A., Tanner K.E. (2008): Characterization and dynamic mechanical analysis of selective laser sintered hydroxyapatite-filled polymeric composites. *Journal of Biomedical Materials Research A*, *86*[3], 607-616. doi: 10.1002/jbm.a.31622.
44. Ruys A.J., Wei M., Sorrell C.C., Dickson M.R., Brandwood A., Milthorpe B.K. (1995): Sintering effects on the strength hydroxyapatite. *Biomaterials*, *16*, 409-415. doi: 10.1016/0142-9612(95)98859-c
45. Azad A.M., Subramaniam T., Dung W. (2002): On the development of high density barium metazirconate ($BaZrO_3$) ceramics. *Journal of Alloys Compounds*, *334*, 118-130. doi: 10.1016/S0925-8388(01)01785-6
46. Pandey A., Nigam V.K., Balani K. (2018): Multi-length scale tribology of hydroxyapatite reinforced with ceria and silver. *Wear*, *404-405*, 12-21. doi: 10.1016/j.wear.2018.01.006
47. Yemisci I., Mutlu O., Gulsoy N., Kunal K., Atrec S., Gulsoy H.O. (2019): Experimentation and analysis of powder injection molded Ti10Nb10Zr alloy: a promising candidate for electrochemical and biomedical application. *Journal of Materials Research and Technology*, *8*[6], 5233-5245. doi: 10.1016/j.jmrt.2019.08.046
48. Ooi C.Y., Hamdi M., Ramesh S. (2007): Properties of hydroxyapatite produced by annealing of bovine bone. *Ceramics International*, *33*[7], 1171-1177. doi: 10.1016/j.ceramint.2006.04.001
49. The British Standards Institution 2018, ISBN 978 0 580 86939-6.
50. Dorozhkin S.V. (2012): Biphasic, triphasic and multiphasic calcium orthophosphates, *Acta Biomaterialia*, *8*, 963-977. doi: 10.1016/j.actbio.2011.09.003
51. Jamil M., Elouahli A., Abida F., Khallok H., Gourri E., Kheribech A., Hatim Z. (2020): Development of triphasic hydroxyapatite/(α and β)-tricalcium phosphate based composites by sintering powder of calcium-apatite in the presence of montmorillonite. *Journal of Inorganic and Organometallic Polymers and Materials*, *30*, 2489-2498. doi: 10.1007/s10904-020-01479-9
52. Kozłowska-Róg A, Bućko M.M, Róg G. (2010): Application of the barium-β”-alumina solid-state electrolyte to the thermodynamic study of the BaO-ZrO_2 system. *Ceramic Materials*, *62*[3], 254-258.
53. Wei-ping G., Teng-fei C., Zhan-peng J. (2007): Thermodynamic investigation of ZrO_2-BaO system. *Transactions of Nonferrous Metals Society of China*, *17*, 232-237. doi: 10.1016/S1003-6326(07)60077-6
54. Kolay S., Basu M., Sudarsan V., Tyagi A.K. (2018): Blue light emitting Eu doped $Ca_2P_2O_7$ and $Ba_2P_2O_7$ particles synthesized at low temperatures. *Solid State Sciences*, *85*, 26-31. doi: 10.1016/j.solidstatesciences.2018.09.007
55. Nakagawa H., Kim S.W., Hasegawa T., Hasegawa S., Ishigaki T., Uematsu K., Toda K., Takaba H., Sato M. (2017): Stabilization of novel high temperature phase yellow-emitting σ-type $(Ba_{1-x-y}Eu_xMg_y)2P_2O_7$ phosphors using a melt synthesis technique. *Inorganic Chemistry Frontiers*, *4*, 1562-1567. doi: 10.1039/C7QI00359E
56. Ozel F., Akman F., Kaçal M.R., Ozen A., Arslan H., Polat H., Yurtcan S., Agar O. (2021): Production of microstructured $BaZrO_3$ and $Ba_2P_2O_7$-based polymer shields for protection against ionizing photons. *Journal of Physics and Chemistry of Solids*, *158*, 110238. doi: 10.1016/j.jpcs.2021.110238
57. Zhen W., Jiang B.J. (2014): Low temperature sintering and microwave dielectric properties of $Ba_3(PO_4)_2$–$BaWO_4$

composite ceramics. *Ceramics International*, *40*[6], 8507-8511. doi: 10.1016/j.ceramint.2014.01.062

58. Zhaozhao W., Rongjuan L., Luyao P., Yang Y., Xiaoguang L., Juncen J., Fan Z. (2021): Easily modified barium phosphate composites for effective removal of methyl blue from solution. *Journal of Environmental Chemical Engineering*, *9*[4], 105423. doi: 10.1016/j.jece.2021.105423
59. Tayyebi S., Mirjalili F., Samadi H., Nemati A. (2015): A review of synthesis and properties of hydroxyapatite/alumina nano composite powder. *Chemistry Journal*, *5*[2], 20-28. ISSN 2049-954X
60. Mezahi F., Harabi A., Zouai S., Achour S., Bernache-Assollant D. (2005): Effect of stabilised ZrO_2, Al_2O_3 and TiO_2 on sintering of hydroxyapatite. *Materials Science Forum*, *492-493*, 241-248. doi: 10.4028/www.scientific.net/MSF.492-493.241
61. Brzezińska-Miecznik J., Haberko K., Sitarz M., Bućko M.M., Macherzyńska B., Lach R. (2016): Natural and synthetic hydroxyapatite/zirconia composites: A comparative study. *Ceramics International*, *42*[9], 11126-11135. doi: 10.1016/j.ceramint.2016.04.019
62. Castkova K., Hadraba H., Matousek A., Roupcova P., Chlup Z., Novotna L., Cihlar J. (2016): Synthesis of Ca, Y-zirconia/hydroxyapatite nanoparticles and composites. *Journal of the European Ceramic Society*, *36*[2], 2903-2912. doi: 10.1016/j.jeurceramsoc.2015.12.045
63. Youness R.A., Taha M.A., Ibrahim M.A. (2020): In vitro bioactivity, molecular structure and mechanical properties of zirconia-carbonated hydroxyapatite nanobiocomposites sintered at different temperatures. *Materials Chemistry and Physics*, *239*, 122011. doi: 10.1016/j.matchemphys.2019.122011
64. Moseke C., Gbureck U. (2010): Tetracalcium phosphate: Synthesis, properties and biomedical applications. *Acta Biomaterialia*, *6*, 3815-3823. doi: 10.1016/j.actbio.2010.04.020
65. Chiba A., Kimura S., Raghukandan K., Morizono Y. (2003): Effect of alumina addition on hydroxyapatite biocomposites fabricated by underwater-shock compaction. *Materials Science and Engineering: A*, *350*[1-2], 179-183. doi: 10.1016/S0921-5093(02)00718-9
66. Abraham C., Devi L.G. (2019): The crucial role of W^{6+}, P^{5+} and N^{3-} dopant ions in the anatase TiO_2 crystal lattice for enhanced photocatalytic activity under the irradiation of UV/ solar light: Structure-reactivity correlation. *Materials Chemistry and Physics*, *229*, 334-347. doi: 10.1016/j.matchemphys.2019.02.061
67. Santoro A., Sora I.N., Huang Q. (2000): Bond valence analysis of $BaRuO_3$. *Journal of Solid State Chemistry*, *151*[2], 245-252. doi: 10.1006/jssc.2000.8647
68. Ye H., Liu X.Y., Hong H. (2009): Characterization of sintered titanium/hydroxyapatite biocomposite using FTIR spectroscopy. *Journal of Materials Science: Materials in Medicine*, *20*, 843-885. doi: 10.1007/s10856-008-3647-3
69. Harabi E., Harabi A., Foughali L., Chehlatt S., Zouai S., Mezahi F.Z. (2015): Grain growth in sintered natural hydroxyapatite. *Acta Physica Polonica A*, *27*[4], 1161-1163. doi: 10.12693/APhysPolA.127.1161
70. Case E.D., Smith I.O., Baumann M.J. (2005): Microcracking and porosity in calcium phosphates and the implications for bone tissue engineering. *Materials Science and Engineering A*, *390*, 246-254. doi: 10.1016/j.msea.2004.08.021
71. Fan X., Case E.D., Ren F., Shu Y., Baumann M.J. (2012): Part I: Porosity dependence of the Weibull modulus for hydroxyapatite and other brittle materials. *Journal of the Mechanical Behavior of Biomedical Materials*, *8*, 21-36. doi: 10.1016/j.jmbbm.2011.12.010
72. Halouani R., Bernache-Assolant D., Champion E., Ababou A. (1994): Microstructure and related mechanical properties of hot pressed hydroxyapatite ceramics. *Journal of Materials Science: Materials in Medicine*, *5*, 563-568. doi: 10.1007/BF00124890
73. Ramli A., Osman N., Othman N.W. (2017): Effect of double heat temperature profile on $Ba(Ce,Zr)O_3$ sintered pellet. *Journal of Engineering and Science Research*, *1*[2], 79-84. doi: 10.26666/rmp.jesr.2017.2.14
74. Sugiyama S., Matsumoto H., Ichii T., Hayashi H., Hiraga Y., Shigemoto N. (2001): Enhancement of lead-barium exchangeability of barium hydroxyapatite. *Journal of Colloid and Interface Science*, *238*[1], 183-187. doi: 10.1006/jcis.2001.7509
75. Sugiyama S., Matsumoto H., Hayashi H., Moffat J.B. (2000): Sorption and ion-exchange properties of barium hydroxyapatite with divalent cations. *Colloids and Surfaces A: Physicochemical and Engineering Aspects*, *169*[1-3], 17-26. doi: 10.1016/S0927-7757(00)00412-X
76. Yasukawa A., Ueda E., Kandori K., Ishikawa T. (2005): Preparation and characterization of carbonated barium-calcium hydroxyapatite solid solutions. *Journal of Colloid and Interface Science*, *288*[2], 468-474. doi: 10.1016/j.jcis.2005.03.007
77. Chiu C.Y., Hsu H.C., Tuan W.H. (2007): Effect of zirconia addition on the microstructural evolution of porous hydroxyapatite. *Ceramics International*, *33*, 715-718. doi: 10.1016/j.ceramint.2005.12.008
78. Oktar F.N., Agathopoulos S., Ozyegin L.S., Gunduz O., Demirkol N., Bozkurt Y., Salman S. (2007): Mechanical properties of bovine hydroxyapatite (BHA) composites doped with SiO_2, MgO, Al_2O_3, and ZrO_2. *Journal of Materials Science: Materials in Medicine*, *18*[11], 2137-2143. doi: 10.1007/s10856-007-3200-9
79. Ke D., Vu A.A., Bandyopadhyay A., Bose S. (2019): Compositionally graded doped hydroxyapatite coating using laser and plasma spray deposition. *Acta Biomaterialia*, *84*, 414-423. doi: 10.1016/j.actbio.2018.11.041
80. Tada H., Kumpel A.E., Lathrop R.E., Slanina J.B., Nieva P., Zavracky P., Miaoulis I.N., Wong P.Y. (2000): Thermal expansion coefficient of polycrystalline silicon and silicon dioxide thin films at high temperatures. *Journal of Applied Physics*, *87*[9], 4189-4193. doi: 10.1063/1.373050
81. Suzuki I. (1975): Thermal expansion of periclase and olivine, and their anhormonic properties. *Journal of Physics of the Earth*, *23*[2], 145-159. doi: 10.4294/jpe1952.23.145
82. Mangalaraja R.V., Chandrasekhar B.K., Manohar P. (2003): Effect of ceria on the physical, mechanical and thermal properties of yttria stabilized zirconia toughened alumina. *Materials Science and Engineering: A*, *343*[1-2], 71-75. doi: 10.1016/S0921-5093(02)00368-4
83. Rendtorff N.M., Suarez G., Sakka Y., Aglietti E.F. (2012): Influence of the zirconia transformation on the thermal behavior of zircon-zirconia composites. *Journal of Thermal Analysis and Calorimetry*, *110*, 695-705. doi: 10.1007/s10973-011-1906-x
84. Xuebin Z., Yunfei D., Songlin W., Jie X., Yi F. (2010): Sintering behavior and kinetic evaluation of hydroxyapatite

bio-ceramics from bovine bone. *Ceramics – Silikáty*, *54*[3], 248-252.

85. Mohammadi M., Tulliani J.M., Montanaro L., Palmero P. (2021): Gelcasting and sintering of hydroxyapatite materials: Effect of particle size and Ca/P ratio on microstructural, mechanical and biological properties. *Journal of the European Ceramic Society*, *41*[4], 7301-7310. doi: 10.1016/j.jeurceramsoc.2021.07.025
86. Indra A., Putra A.B., Handra N., Fahmi H., Asfarizal N., Perdana M., Subardi A., Affi J., Behavior of sintered body properties of hydroxyapatite ceramics: Effect of uniaxial pressure on green body fabrication. *Materials Today Sustainability*, *17*, (2022) 100100. Doi: 10.1016/j.mtsust.2021.100100
87. Rao R.R. Kannan T.S. (2002): Synthesis and sintering of hydroxyapatite-zirconia composites. *Materials Science and Engineering: C*, *20*[1-2], 187-193. doi: 10.1016/S0928-4931(02)00031-0
88. John S.T., Irvine T.S. (2007): Conductivity studies of dense yttrium-doped $BaZrO_3$ sintered at 1325 °C. *Journal of Solid State Chemistry*, *180*[12], 3493-3503. doi: 10.1016/j.jssc.2007.09.027
89. Chernaya V.V., Shpanchenko R.V., Velikodnyi Y.A., Kovba M.L., Antipov E. V. (2006): Crystal structure of the pyrovanadate $K_4V_2O_7$. *Russian Journal of Inorganic Chemistry*, *51*[5], 779-784. doi: 10.1134/S0036023606050159
90. Elbelghitti A.A., Elmarzouki A., Boukhari A., Holt E.M. (1995): σ-dibarium pyrophosphate. *Acta Crystallographica* Section C *Structural Chemistry*, 51 (1995) 1478-1480. doi: 10.1107/S0108270195001739
91. Ianoş R., Barvinschi P. (2010): Solution combustion synthesis of calcium zirconate, $CaZrO_3$, powders. *Journal of Solid State Chemistry*, *183*[3], 491-496. doi: 10.1016/j.jssc.2009.12.015
92. Ozeki K., Fukui Y., Aoki H. (2007): Influence of the calcium phosphate content of the target on the phase composition and deposition rate of sputtered films. *Applied Surface Science*, *253*[11], 5040-5044. doi: 10.1016/j.apsusc.2006.11.011
93. Ahmad N., Tsuru K., Munar M.L., Maruta M., Matsuya S., Ishikawa K. (2012): Effect of precursor's solubility on the mechanical property of hydroxyapatite formed by dissolution-precipitation reaction of tricalcium phosphate. *Dental Materials Journal*, *31*[6], 995-100. doi: 10.4012/dmj.2012-176
94. Hung I.M., Shih W.J., Hon M.H., Wang M.C. (2012): The properties of sintered calcium phosphate with [Ca]/[P] = 1.50. *International Journal of Molecular Science*, *13*[10], 13569-13586. doi: 10.3390/ijms131013569
95. Aminzare M., Eskandari A., Baroonian M.H., Berenov A., Hesabi Z.R., Taheri M., Sadrnezhaa S.K. (2013): Hydroxyapatite nanocomposites: Synthesis, sintering and mechanical properties. *Ceramics International*, 39, 2197-2206. doi: 10.1016/j.ceramint.2012.09.023
96. Chen P.Y., Wang S.F., Chien R.R., Tu C.S., Feng K.C., Chen C.S., Hung K.Y., Schmidt V.H. (2019): Evolution of the microstructural and mechanical properties of hydroxyapatite bioceramics with varying sintering temperature. *Ceramics International*, *45*[13], 16226-16233. doi: 10.1016/j.ceramint.2019.05.144
97. Jodati H., Tezcaner A., Alshemary A.Z., Şahin V., Evis Z. (2022): Effects of the doping concentration of boron on physicochemical, mechanical, and biological properties of hydroxyapatite. *Ceramics International*, *48*[16], 22743-22758. doi: 10.1016/j.ceramint.2022.04.058
98. Nie J., Zhou J., Huang X., Wang L., Liu G., Cheng J. (2019): Effect of TiO_2 doping on densification and mechanical properties of hydroxyapatite by microwave sintering. *Ceramics International*, *45*[11], 13647-13655. doi: 10.1016/j.ceramint.2019.04.007
99. Dasgupta S., Tarafder S., Bandyopadhyay A., Bose S. (2013): Effect of grain size on mechanical, surface and biological properties of microwave sintered hydroxyapatite. *Materials Science and Engineering: C*, *33*[5], (2013) 2846-2854. doi: 10.1016/j.msec.2013.03.004
100. Khiri M.Z.A., Matori K.A., Zaid M.H.M., Abdullah C.A.C., Zainuddin N., Alibe I.M., Rahman N.A.A., Wahab S.A.A., Azman A.Z.K., Effendy N. (2019): Crystallization behavior of low-cost biphasic hydroxyapatite/β-tricalcium phosphate ceramic at high sintering temperatures derived from high potential calcium waste sources. *Results in Physics*, *12*, 638-644. doi: 10.1016/j.rinp.2018.12.025
101. Hannora A.E. (2014): Preparation and characterization of hydroxyapatite/alumina nanocomposites by high-energy vibratory ball milling. *Journal of Ceramic Science and Technology*, *5*[4], 293-298. doi: 10.4416/JCST2014-00019
102. Rice R.W., Wu C.C., Borchelt F. (1994): Hardness-grain-size relations in ceramics. *Journal of the American Ceramic Society*, *77*[10], 2539-2553. doi: 10.1111/j.1151-2916.1994.tb04641.x
103. Wang J., Shaw L.L. (2009): Nanocrystalline hydroxyapatite with simultaneous enhancements in hardness and toughness. *Biomaterials*, *30*[34], 6565-6572. doi: 10.1111/j.1151-2916.1994.tb04641.x
104. Hoepfner T.P., Case E.D. (2003): The influence of the microstructure on the hardness of sintered hydroxyapatite. *Ceramics International*, *29*[6], (2003) 699-706. doi: 10.1016/S0272-8842(02)00220-1
105. Hervas I., Montagne A., Gorp A.V., Bentoumi M., Thuault A., Iost A. (2016): Fracture toughness of glasses and hydroxyapatite: A comparative study of 7 methods by using Vickers indenter. *Ceramics International*, *42*[11], 12740-12750. doi: 10.1016/j.ceramint.2016.05.030
106. Lin K., Chen L., Chang J. (2012): Fabrication of dense hydroxyapatite nano bioceramics with enhanced mechanical properties via two-step sintering process. *International Journal of Applied Ceramic Technology*, *9*[3], 479-485. doi: 10.1111/j.1744-7402.2011.02654.x
107. Ramesh S., Aw K.L., Tolouei R., Amiriyan M., Tan C.Y., Hamdi M., Purbolaksono J., Hassan M.A., Teng W.D. (2013): Sintering properties of hydroxyapatite powders prepared using different methods. *Ceramics International*, *39*, 111-119. doi: 10.1016/j.ceramint.2012.05.103
108. Gu Y.W., Loh N.H., Khor K.A., Tor S.B., Cheang P. (2002): Spark plasma sintering of hydroxyapatite powders. *Biomaterials*, *23*[1], 37-43. doi: 10.1016/S0142-9612(01)00076-X
109. White A.A., Best S.M. (2007): Hydroxyapatite-carbon nanotube composites for biomedical applications: A Review. *International Journal of Applied Ceramic Technology*, *4*[1], 1-13. doi: 10.1111/j.1744-7402.2007.02113.x
110. Kobayashi S., Kawai W., Wakayama S. (2006): The effect of pressure during sintering on the strength and the fracture toughness of hydroxyapatite ceramics. *Journal of*

Materials Science: Materials in Medicine, *17*, 1089-1093. doi: 10.1007/s10856-006-0535-6

111. Lopes M.A., Monteiro F.J., Santos J.D. (1999): Glass-reinforced hydroxyapatite composites: fracture toughness and hardness dependence on microstructural characteristics. *Biomaterials*, *20*[21], 2085-2090. doi: 10.1016/S0142-9612(99)00112-X
112. Aguirre T.G., Cramer C.L., Torres V.P., Hammann T.J., Holland T.B., Ma K. (2019): Effects of the addition of boron nitride nanoplate on the fracture toughness, flexural strength, and weibull distribution of hydroxyapatite composites prepared by spark plasma sintering. *Journal of the Mechanical Behavior of Biomedical Materials*, *93*, 105-117. doi: 10.1016/j.jmbbm.2019.01.021
113. Ramesh S., Tan C.Y., Peralta C.L., Teng W.D. (2007): The effect of manganese oxide on the sinterability of hydroxyapatite. *Science and Technology of Advanced Materials*, *8*[4], 257-263. doi: 10.1016/j.stam.2007.02.006
114. Gautam C.R., Kumar S., Biradar S., Josec S., Mishra V.K. (2016): Synthesis and enhanced mechanical properties of MgO substituted hydroxyapatite: a bone substitute material. *RSC Advances*, 6, 67565-67574. doi: 10.1039/c6ra10839c
115. Goller G., Demirkıran H., Oktar F.N., Demirkesen E. (2003): Processing and characterization of bioglass reinforced hydroxyapatite composites. *Ceramics International*, *29*[6], 721-724. doi: 10.1016/S0272-8842(02)00223-7
116. Pal A., Metya A.K., Chowdhury A.R., Sinha A. (2020): Structural and mechanical behavior of mechanochemically synthesized nanocrystalline hydroxyapatite from mercenaria clam shells. *Transactions of the Indian Ceramic Society*, *79*[4], 175-181. doi: 10.1080/0371750X.2020.1792806
117. Shaly A.A., Priya G.H., Linet J.M. (2020): An outlook on the mechanical attributes and load curve analysis of hydrothermally acquired hydroxyapatite bioceramic nanoparticles. *Physica B: Condensed Matter*, *590*, 41223. doi: 10.1016/j.physb.2020.412223
118. Bianco A., Cacciotti I., Lombardi M., Montanaro L., Bemporad E., Sebastiani M. (2010): F-substituted hydroxyapatite nano powders: Thermal stability, sintering behaviour and mechanical properties, *Ceramics International*, *36*[1], 313-322. doi: 10.1016/j.ceramint.2009.09.007
119. Saxena V., Hasan A., Pandey L.M. (2018): Effect of Zn/ZnO integration with hydroxyapatite: a review. *Materials Technology*, *33*[2], 79-92. doi: 10.1080/10667857.2017.1377972
120. Shi S.L., Pan W. (2007): Machinable Ti_3SiC_2/Hydroxyapatite bioceramic composites by spark plasma sintering. *Journal of the American Ceramic Society*, *90*[10], 3331-3333. doi: 10.1111/j.1551-2916.2007.01882.x
121. Shaly A.A., Priya G.H., Mahendiran M., Linet J.M. (2022): A behavioural study of hydrothermally derived novel alumina/magnesia/hydroxyapatite (Al_2O_3/MgO/HA) bioceramic nanocomposite. *Journal of the Mechanical Behavior of Biomedical Materials*, *133*, 105313. doi: 10.1016/j.jmbbm.2022.105313
122. Shaly A.A., Priya G.H., Mahendiran M., Linet J.M., Mani J.A.M. (2022): An intrinsic analysis on the nature of alumina (Al_2O_3) reinforced hydroxyapatite nanocomposite. *Physica B: Condensed Matter*, *642*, 414100. doi: 10.1016/j.physb.2022.414100
123. Qiao Z., Li S., Li Y., Wang J. (2021): Properties of barium zirconate sintered from different barium and zirconium sources. *Ceramics International*, *47*[22], 31194-31201. doi: 10.1016/j.ceramint.2021.07.295
124. Vassal M.F., Nunes-Pereira J., Miguel S.P., Correia I.J., Silva A.P. (2019): Microstructural, mechanical and biological properties of hydroxyapatite-$CaZrO_3$ biocomposites. *Ceramics International*, *45*[7], 8195-8203. doi: 10.1016/j.ceramint.2019.01.122
125. Nawang R., Hussein M.Z., Matoria K.A., Abdullah C.A.C., Hashim M. (2019): Physicochemical properties of hydroxyapatite/montmorillonite nanocomposite prepared by powder sintering. *Results in Physics*, *15*, 102540. doi: 10.1016/j.rinp.2019.102540
126. Khalil K.A., Kim S.W., Kim H.Y. (2007): Consolidation and mechanical properties of nanostructured hydroxyapatite-(ZrO_2+3mol% Y_2O_3) bioceramics by high-frequency induction heat sintering. *Materials Science and Engineering: A*, *456*[1-2], 368-372. doi: 10.1016/j.msea.2006.12.005
127. Hincapie-Bedoya J., Poblano-Salas C.A., Moreno-Murguia B., Gutierrez-Perez A.I., Henao J., Espinosa-Arbelaez D.G., Giraldo-Betancur A.L. (2022): Effect of the modification of spray drying parameters on the fabrication of bovine-derived hydroxyapatite microspheres for biomedical applications. *Materials Today Communications*, 31, 103838. doi: 10.1016/j.mtcomm.2022.103838
128. Precnerová M., Bodišová K., Frajkorová F., Galusková D., Nováková Z.V., Vojtaššák J., Lenčéš Z., Šajgalík P. (2015): In vitro bioactivity of silicon nitride-hydroxyapatite composites. *Ceramics International*, *41*[6], 8100-8108. doi: 10.1016/j.ceramint.2015.03.011
129. Chern Lin J.H., Lin, H.J., Ding S.J., Ju, C.P. (2000): Characterization of immersed hydroxyapatite-bioactive glass coatings in Hank's solution. *Materials Chemistry and Physics*, *64*[3], 229-240. doi: 10.1016/S0254-0584(00)00209-1
130. Quan R., Tang Y., Huang Z., Xu J., Wu X., Yang D. (2013): Study on the genotoxicity of HA/ZrO_2 composite particles in vitro. *Materials Science and Engineering:* C, *33*[3], 1332-1338. doi: 10.1016/j.msec.2012.12.033
131. Webster T.J., Ergun C., Doremus R.H., Siegel R.W., Bizios R. (2000): Specific proteins mediate enhanced osteoblast adhesion on nanophase ceramics. *Journal of Biomedical Materials Research*, *51*[3], 475-483. doi: 10.1002/1097-4636(20000905)51:3<475::AID-JBM23>3.0.CO;2-9open_in_newPublisherJ
132. Bose S., Dasgupta S., Tarafder S., Bandyopadhyay A. (2010): Microwave-processed nanocrystalline hydroxyapatite: simultaneous enhancement of mechanical and biological properties. *Acta Biomaterialia*, *6*[9], 3782-3790. doi: 10.1016/j.actbio.2010.03.016